sustainability

MDPI

Article

Reactivity Effect of Calcium Carbonate on the Formation of Carboaluminate Phases in Ground Granulated Blast Furnace Slag Blended Cements

Walid Deboucha [1,*], Nassim Sebaibi [1], Yassine El Mendili [1], Aurélie Fabien [1], U. Johnson Alengaram [2], Nordine Leklou [3], Mahmoud N Hamdadou [3], Alexandra Bourdot [4] and Stéphanie Gascoin [5]

1 COMUE NU, Laboratoire de Recherche ESITC Caen, 1 Rue Pierre et Marie Curie, 14610 Epron, France; nassim.sebaibi@esitc-caen.fr (N.S.); yassine.el-mendili@esitc-caen.fr (Y.E.M.); aurelie.fabien@esitc-caen.fr (A.F.)
2 Centre for Innovative Construction Technology, Department of Civil Engineering, Faculty of Engineering, University of Malaya, Kuala Lumpur 50603, Malaysia; johnson@um.edu.my
3 LUNAM University, University of Nantes-IUT Saint-Nazaire, GeM, CNRS UMR 6183, 44600 Saint-Nazaire, France; nordine.leklou@univ-nantes.fr (N.L.); mahmoud-nacer-eddine.hamdadou@etu.univ-nantes.fr (M.N.H.)
4 LMT-Laboratoire de Mécanique et Technologie, Université Paris-Saclay, ENS Paris-Saclay, CNRS, 91190 Gif-sur-Yvette, France; alexandra.bourdot@ens-paris-saclay.fr
5 CRISMAT-ENSICAEN, UMR CNRS 6508, Normandie Université, 6 Boulevard Maréchal Juin, 14050 Caen, France; Stephanie.gascoin@ensicaen.fr
* Correspondence: walid.deboucha@esitc-caen.fr

Abstract: The reactivity effect of calcium carbonate, present in ground oyster shells and limestone filler, on the formation of carboaluminate phases in ground granulated blast furnace slag blended cement pastes was reported in this paper. Six different binary and ternary blended cement pastes were prepared using ground granulated blast furnace slag, ground oyster shells and limestone filler with different replacement levels (from 5 to 35%). The carboaluminate formation was assessed and quantified directly using X-ray diffraction (XRD), and indirectly by following the aluminate phase's reaction (heat flow) and consumed calcium carbonate using Isothermal Calorimetry (IC) and Thermogravimetric Analysis (TGA), respectively. Further, the overall reaction degree calculated based on TGA results and the compressive strength were determined to support the findings obtained. The results revealed that the calcium carbonate present in ground oyster shells is more reactive when compared to that present in limestone filler, where more formed hemi- and monocarboaluminate phases were observed in mixtures containing ground oyster shells. An enhancement in compressive strength and overall reaction degree was observed by adding 5% ground oyster shells as cement replacement.

Keywords: oyster shells; limestone filler; slag; calcium carbonate; carboaluminate phases formation

Citation: Deboucha, W.; Sebaibi, N.; El Mendili, Y.; Fabien, A.; Alengaram, U.J.; Leklou, N.; Hamdadou, M.N.; Bourdot, A.; Gascoin, S. Reactivity Effect of Calcium Carbonate on the Formation of Carboaluminate Phases in Ground Granulated Blast Furnace Slag Blended Cements. *Sustainability* **2021**, *13*, 6504. https://doi.org/10.3390/su13116504

Academic Editor: José Ignacio Alvarez

Received: 7 May 2021
Accepted: 3 June 2021
Published: 7 June 2021

1. Introduction

The need for reducing energy consumption and CO_2 emission caused by cement production has become an increasingly important issue in recent years [1–4]. The use of mineral additives as clinker or as cement replacement should help in achieving environmental and economic advantages [5,6], and should also help in achieving the required technical performance [7,8].

Mineral additives, natural or byproduct materials, are widely used in blended cement systems to improve the chemical properties, i.e., hydration reactions, the mechanical properties such as strength, and the durability of concretes [9,10]. Among mineral additives used, ground granulated blast furnace slag (GGBFS), fly ash (FA), and limestone filler (LF) are the most commonly used for cement replacement. The main advantage of the use of LF is the early ages compressive strength improvement by enhancing the hydration rate

through its filler effect [11,12]. GGBFS is used generally to increase workability, decrease the hydration heat at early ages, and to improve the durability of concrete [11,13–15]. However, the main weakness of using GGBFS in blended cement is the low short-term compressive strength of concretes due to its latent hydration reaction [16]. Chemical, thermal, and mechanical activations were used to accelerate the hydration processes of GGBFS [17–21]. These activation methods, however, seem limited and have negative impacts on some concrete properties. For instance, the mechanical activation (increasing in the fineness degree) of GGBFS generates early ages microcracking caused by self-desiccation shrinkage [22]. Early-age microcracking leads to higher permeability and consequently reduces concrete durability [22]. In addition, the chemical and thermal activations of GGBFS using alkali-activated solutions, i.e., sodium silicate solution, and heat treatment increase the overall cost of concrete production [23]. Hence, providing another method to accelerate and activate the hydration processes of GGBFS is needed. An emerging solution that consists in the possibility of activating the hydration processes of GGBFS by using other mineral additives such as LF has gained much considerable interest [24–27]. Recently, it was demonstrated that the addition of LF to GGBFS blended cement improves hydration reactions through its filler and chemical effects [25,26]. The filler effect manifests itself in two ways: dilution effect and heterogeneous nucleation effect. The chemical (activation effect) consists in the ability of calcium carbonate ($CaCO_3$), present in limestone filler to react with aluminate phases of GGBFS to form hemi- and monocarboaluminate phases. The formation of hemi- and monocarboaluminate phases leads to increasing hydrates' volume and thus improving the compressive strength [25–27].

Oyster shells (OS) are seashell waste which are available in huge amounts in some countries and are usually rejected or landfilled without any valorization [28,29]. The use of this material as a raw material in concrete should help in achieving environmental, technical and economic advantages. Studies have been carried out to study the possibility of the use of OS as fine aggregate, coarse aggregate and even as cement replacement in concrete and mortar [30–34]. Most of the previous studies were related to the effect of using OS as an aggregate on concrete properties. Only few studies have focused on the effect of OS as a cement replacement on concrete properties [29]. Liu et al. [30] reported that the use of treated oyster shells as fine aggregate improved the durability of concrete. They found that the use of oyster shells treated with polyvinyl alcohol and sodium silicate reduced water permeability and chloride migration coefficients. Kuo et al. [35] found that the use of 5% crushed oyster shells as a sand replacement improved the compressive strength of mortar by about 5% compared to that of reference mortar. However, a decrease in compressive strength was noticed beyond this replacement level. Zhong et al. [36] found that the use of 5% GOS as a cement replacement exhibited an enhancement in compressive strength by about 5% compared to the compressive strength of reference cement mortar.

GOS are composed primarily calcium carbonate. Their chemical composition is similar to LF [29], which makes it possible to use GOS as an activator for the hydration processes of GGBFS. In fact, the calcium carbonate present in GOS is expected to react with aluminate phases of GGBFS to form hemi- and monocarboaluminate phases. Moreover, the average diameters of calcium carbonate particles present in GOS is smaller to that present in LF which means that the calcium carbonate present in GOS may react more to that present in LF.

The reactivity effect of calcium carbonate on the formation of carboaluminate phases is the aim of the current study. For this purpose, LF with a calcium carbonate content of ~96.5% and (GOS) with calcium carbonate content of about 99% were used and added to GGBFS Blended cements. Isothermal Calorimetry (IC), Thermogravimetric Analysis (TGA), and X-ray diffraction (XRD) were used to assess and quantify the carboaluminate phases' formation. The overall reaction degree of blended cement pastes investigated was also evaluated using the method suggested in [27,37] which were based on TGA results. Those techniques were completed by compressive strength to further justify and verify the findings obtained.

2. Materials and Methods

2.1. Materials

2.1.1. Cement

The cement used in the current study is Portland cement Type I CEM I 52.5 N provided by Vicat company (Bourgoin, France). The fineness of this cement is 4500 cm^2/g. Its mineralogical composition is 12.1% C_2S, 66.9% C_3S, 1% C_3A and 15% C_4AF. The chemical composition and the physical properties provided by the manufacturer are given in Table 1.

Table 1. Chemical composition and physical properties of CEM I 52.5 N and GGBFS.

Chemical Composition (%)	OPC	GGBFS
SiO_2	21.57	37.3
Al_2O_3	3.50	10.7
Fe_2O_3	5.27	0.2
CaO	64.31	43
MgO	1.44	6.5
SO_3	2.25	0.1
K_2O	/	0.35
Na_2O	0.55	0.23
LOI	0.86	1.5
Physical properties		
Density (g/cm^2)	3.22	2.9
Initial setting time (min)	215	/
Final setting time (min)	/	335
Expansion (mm)	1	/

2.1.2. Ground Granulated Blast Furnace Slag

GGBFS used in this study was obtained from local industry (Ecocem, France). The Blaine fineness and the density of GGBFS are 4450 cm^2/g and 2.9 g/cm^3, respectively. Its chemical composition is given in Table 1.

2.1.3. Limestone Filler

The first mineral additive used to activate the hydration processes of GGBFS is limestone filler. The LF used was provided by Omya International AG company (Aucrais, France). The calcium carbonate content determined by X-ray diffraction, the Blaine fineness, the density, and the water content of LF are 96.5%, 4670 cm^2/g, 2.7 g/cm^3 and 0.2%, respectively.

2.1.4. Oyster Shells

The second mineral additive used to activate the hydration processes of GGBFS is oyster shells. Oyster shells are seashell waste collected from a local company (Ovive, France), after being washed (to remove organic residues on the surface) and crushed (Figure 1a). The raw oyster shells obtained were dried in a dry oven at 105 °C and then ground in a laboratory mill to obtained Blaine finesse close to that of cement; LF and GGBFS used (Figure 1b). The Blaine fineness and the density of ground oyster shells (GOS) are 4500 cm^2/g and 2.7 g/cm^3, respectively. They calcium carbonate content determined by X-ray diffraction is about 99%.

(**a**) (**b**)

Figure 1. Oyster shells. (**a**) before grinding; (**b**) after grinding.

2.2. Mixture Proportion

Apart from reference cement paste, the Portland cement CEM I 52.5 N was replaced by GGBFS, LF, and GOS to obtain six different binary and ternary blended cement pastes. For binary blended cements pastes, the replacement level of cement by LF or GOS was selected at 5% by mass based on previous studies [26], where an enhancement in hydration degree and compressive strength was observed when cement is replaced by 5% LF. For ternary blended cements pastes, the cement was replaced by GGBFS and LF or GOS at replacement levels of 25 and 35%, respectively. The water to binder ration was selected at 0.48. The mixture nomenclatures and their proportion based on the replacement of cement by GGBFS, LF, and GOS are given in Table 2.

Table 2. Mix details of blended cement pastes (kg/m^3).

Mix	Cement kg/m^3	GGBFS kg/m^3	LF kg/m^3	GOS kg/m^3	Water kg/m^3
PREF	1265	/	/	/	607
P5LF	1200	/	63.2	/	606
P5GOS	1200	/	/	63.2	606
P5LF20BFS	1001	253	63.2	/	632.7
P5LF30BFS	925.4	379.4	63.2	/	656.7
P5GOS20BFS	1001	253	/	63.2	632.7
P5GOS30BFS	925.4	379.4	/	63.2	656.7

2.3. Methods

Blended cement pastes were prepared, cast, and cured under similar conditions to that of mortar given by EN NF 196-1 [38]. Isothermal Calorimetry (IC), Thermogravimetric Analysis (TGA) and X-ray diffraction (XRD) were used to assess and quantify the carboaluminate phases formation. The compressive strength test was performed to justify and verify the finding. For XRD and TGA tests, the samples specimens after casting were placed in plastic vials hermetically closed. The sample specimens were then stored at 20 °C room temperature. For the compressive strength test, paste samples were cast into $4 \times 4 \times 16$ cm^3 steel molds. After 24 h of casting, paste samples were then demolded and immersed in a water tank at ambient temperature.

2.3.1. Isothermal Calorimetry (IC)

At early ages, the carboaluminate phases formation was evaluated through the GGBFS's aluminate phases interaction with calcium carbonate contained in LF or GOS. the GGBFS's aluminate phases reaction assessment was achieved by measuring the heat flow resulting from the chemical reaction using an 8-channel isothermal calorimeter device (TAM AIR). Blended cement pastes weighing 4–6 g were placed directly after mixing into

standard plastic vials and then loaded into the channel isothermal calorimeter. The heat flow measurements were continued for about 168 h (7 days).

2.3.2. X-ray Diffraction (XRD)

X-ray powder diffraction data were recorded at room temperature on a D8 Advance Vario 1 Bruker (two-circle diffractometer, θ–2θ Bragg-Brentano mode) using a pure copper Kα radiation (λ = 1.54059 Å) selected by an incident beam Ge (111) monochromator. Data were collected from 5° to 100° for 1 s per 0.01° step (2θ varying, 4 h/scan). LaB_6 standard powder (NIST SRM-660b) was used to calibrate the instrumental [39]. For LF and GOS powders, crystalline phases identification was performed using the Full-Pattern Search-Match procedure and the Crystallography Open Database [40]. Rietveld refinement was also performed using the MAUD software to quantify the crystalline phases [41].

2.3.3. Thermogravimetric Analysis (TGA)

TGA test was performed after 3, 7 and 28 days of curing time on crushed and sieved paste specimens using NETZSCH STA 449 F5 device. Specimens were heated up to 1000 °C at a heating rate of 5 °C/min under an N_2 environment. Using this technique, the reactivity of LF and GOS was established by quantifying the consumption of calcium carbonate present in these mineral additives. The direct quantification of the carboaluminate phases formation using this technique is complicated, as the decomposition of other cement hydrate products is in the same temperature range.

Using this technique, the overall reaction degree of blended cement pastes studied was also calculated to establish the carboaluminate phases formation, since the hemi- and mono-carboaluminate formation results in the increase of hydrates' volume, thus increasing the reaction degree. The overall reaction degree was calculated using a methodology suggested in Refs. [27,37]. The chemically bound water content (W_B) and the reaction degree (α) were calculated based on the mass loss between 140 and 1000 °C using Equations (1) and (2).

$$W_B = Ldh + Ldx + 0.41\,(Ldc\text{-}Ldc_a) - (m_c \times LOIcc + M_{A1} \times LOI_{AC1} + M_{A2} \times LOI_{AC2}) + md \quad (1)$$

where Ldh, Ldx, and Ldc are the mass loss on TGA curves within the temperature ranges of 140–400 °C, 400–600 °C and 600–800 °C, respectively. Ldc_a, m_c, m_{A1}, and m_{A2} are the mass loss within the temperature range of 600–800 °C during TGA tests on used anhydrous materials (GGBFS, LF, GOS and cement), and the mass of anhydrous materials contained in the sample, respectively. LOI_{ACC}, LOI_{AC1}, LOI_{AC2} are the losses on ignition corrected for cement, first mineral additive used (GGBFS) and second mineral additives used (LF or GOS), respectively, after subtracting the mass loss between 600 and 800 °C on TGA curves (the mass loss between 105 and 600 °C during TGA tests on anhydrous materials). Md is the device's drift (md). Parameters of Equation (1) are defined and described in detail in [27].

$$\alpha = W_B/W_{B\infty} \times (mc + K_1 \times m_{A1} + K_2 \times m_{A2}) \quad (2)$$

where $W_{B\infty}$, K_1 and K_2 are the ultimate chemically bound water, the activity coefficient of the first and the second mineral additive used, respectively. The activity coefficients for GGBFS and LF, given by EN NF 206-1 [42], are 0.9 and 0.25, respectively. The activity coefficient for GOS was determined according to Equation (3) [27], where 'I' is the 28 days compressive strength ratio of cement mortar made with 25% GOS to that of pure cement mortar. The activity coefficient of GOS determined was slightly higher (0.28) than the one of limestone filler.

$$K = 3 \times I - 2 \quad (3)$$

2.3.4. Compressive Strength Test

After a flexural strength test on 4 × 4 × 16 cm^3 using a flexural-compressive testing machine at a loading rate of 0.05 kN/s confirming to NF EN 196-1 [38], a compressive strength test was carried out on six 4cm-edge cubes using same testing machine but at a

loading rate of 2.4 kN/s. The compressive strength test was performed after 3, 7 and 28 days of curing time. The compressive strength test was performed to justify the finding obtained.

3. Results

The carboaluminate phases formation was followed and quantified directly using XRD test and indirectly by following the aluminate phase's reaction (heat flow) and consumed calcium carbonate using Isothermal Calorimetry and Thermogravimetric Analysis.

3.1. Heat Flow

For the first hours of hydration, the interaction between aluminate phases of GGBFS and calcium carbonate contained in LF or GOS to form carboaluminate phases was followed by measuring the heat flow using Isothermal calorimeter TAM AIR device. Figure 2a,b show the heat flow of binary and ternary cement pastes studied. The heat flow curves present the silicate and aluminate phases' cement hydration [25,26]. The first peak (I) corresponds to the hydration of silicate phases. The second (II) concerns the hydration of aluminate phases.

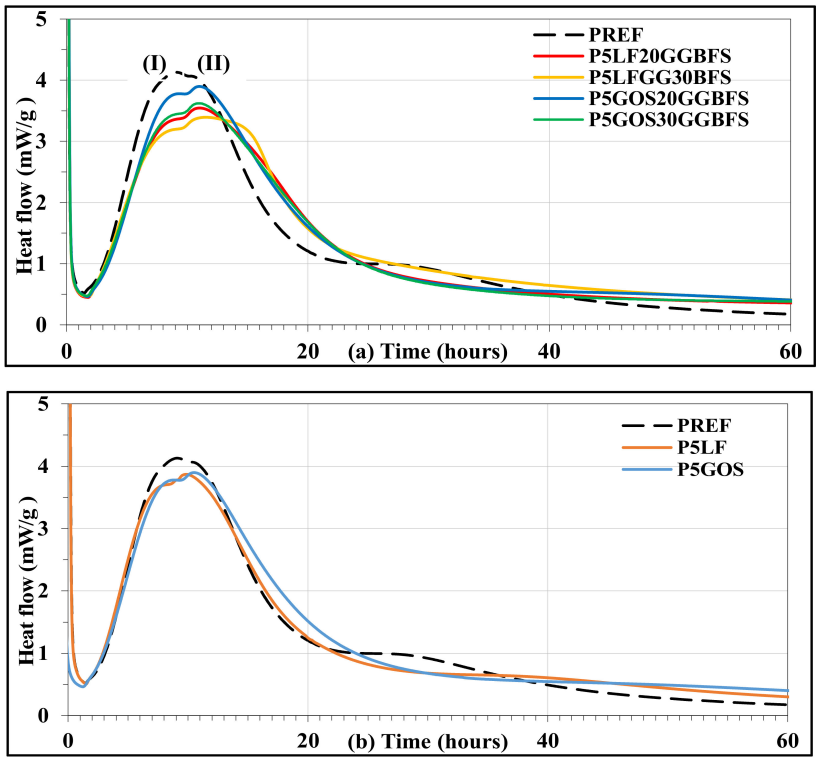

Figure 2. Heat flow of (**a**) ternary cement pastes; (**b**) binary cement pastes.

In the reference cement paste, the first peak that corresponds to the silicate hydration is higher than the one of aluminate hydration. The lowest aluminate phases hydration in reference cement paste is due to the high silicate content in the cement used (Table 1). An opposite trend, however, was observed in ternary cement pastes where the second peak corresponding to the aluminate phases hydration was dominant. This change is due directly to the reaction of aluminate phases with carbonate calcium to form hemi- and monocarboaluminate [27]. Moreover, it is clear from the heat flow curves presented in Figure 2a that the second peak is more dominant in cement pastes prepared with GGBFS and GOS, compared to the second peak in cement pastes prepared with GGBFS and LF. This confirms that the carbonate calcium from GOS reacts more with aluminate phases of GGBFS, thus leading to the formation of more carboaluminate phases. This finding is verified and justified by XRD and TGA tests as shown in the next sections.

Figure 2b shows the heat flow curves for binary cement pastes prepared with GOS and LF. As shown in this Figure, the addition of GOS or LF to cement improves the cement's

aluminate phase hydration where the second peak intensity is higher to that of the primary peak. The higher second peak intensity was obtained with GOS cement paste which reflects a better hydration reaction between cement's aluminate phase and calcium carbonate present in GOS.

3.2. Carboaluminate Phases Formation

A direct assessment of hemi- and monocarboaluminate phases formation was conducted using XRD test after 3, 7 and 28 days of hydration. Figure 3 depicts XRD patterns and identified phases within 2θ range of 5–12 °C.

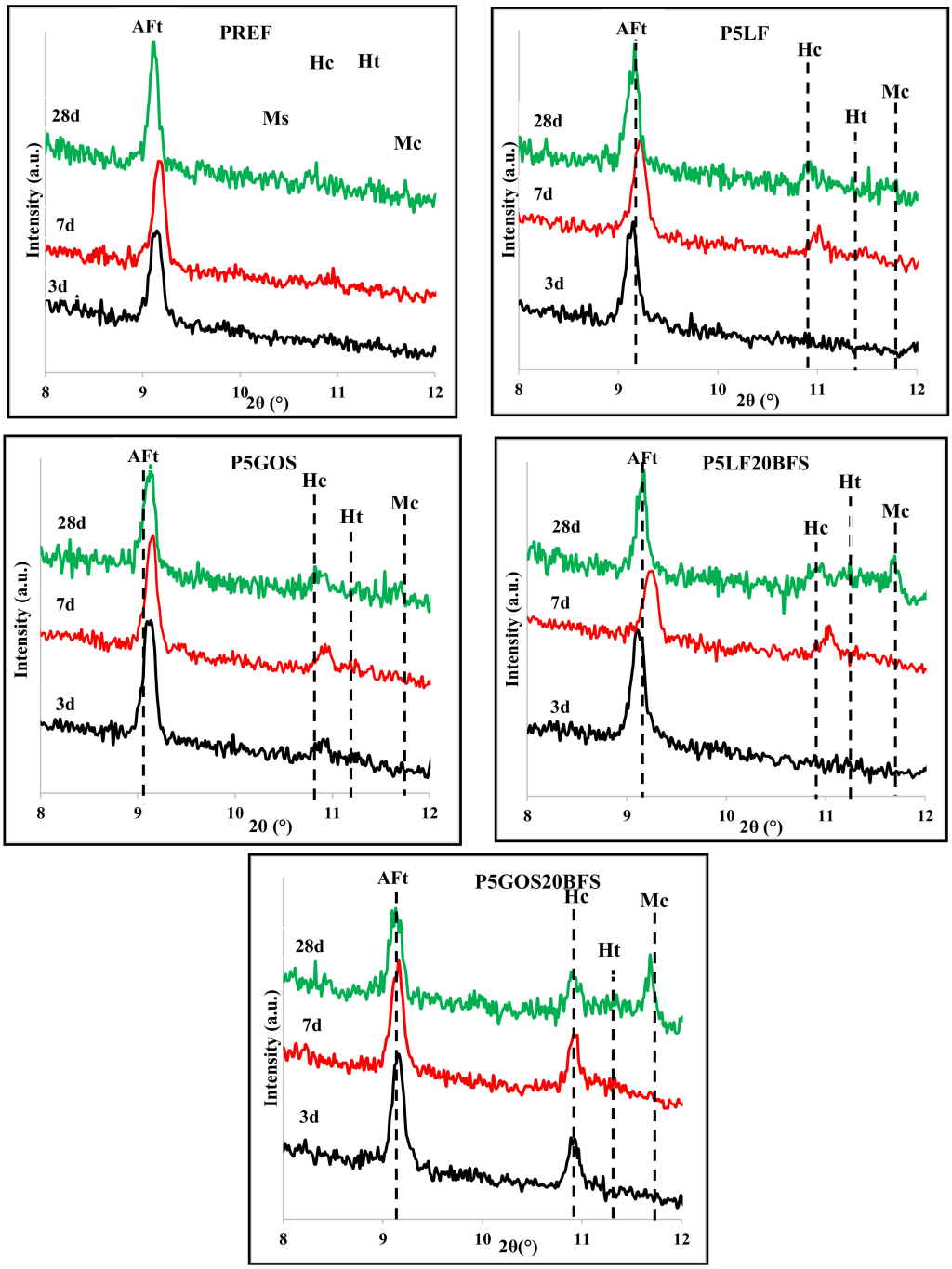

Figure 3. XRD patterns and identified phases within 2θ range of 5–12 °C for binary and ternary cement pastes studied. Aft-ettringite, Hc- Hemicarboaluminate, Mc-monocarboaluminate.

For all cement pastes studied and for all testing ages, the main cement hydrate product, within 2θ range of 5–12 °C, is the ettringite (AFt) as shown in Figure 3. After the first 3 days of hydration, more ettringite was formed in binary and ternary blended cement pastes compared to the reference cement paste, which is due to the presence of LF or GOS. Indeed, the addition of LF or GOS to cement improves hydration rates through their filler effect [37].

The presence of carboaluminate phases is evident from XRD patterns in Figure 3, particularly for binary and ternary mixes. For the reference cement paste, the carboaluminate phases were observed only after 28 days of hydration with lower reflection.

For binary and ternary cement pastes studied (P5LF, P5GOS, P5LF20BFS and P5GOS20BFS), the main carboaluminate phase is the hemicarboaluminate with higher reflection intensities in cement pastes containing GOS at all ages. This means that more carboaluminate phases were formed in cement pastes containing GOS due to the high reactivity of calcium carbonate present in GOS. The hemicarboaluminate reflex is not visible after 3 days of hydration in cement paste containing LF. This might be due to the low reactivity of calcium carbonate present in LF. The monocarboaluminate was observed after 28 days of hydration with higher reflection intensities in ternary cement pastes, particularly for GOS and GGBFS mix. Similar findings for GGBFS and LF ternary mix were reported by Adu-Amankwah et al. [26]. They observed that the hemicarboaluminate forms first, followed by the monocarboaluminate. Furthermore, they observed that the LF content influenced the carboaluminate phases formation, where a higher monocarboaluminate contents was revealed in ternary mixes with high LF content (20%).

3.3. Consumption of Calcium Carbonate

The reactivity of calcium carbonate present in GOS and LF was also evaluated by measuring the consumed calcium carbonate. The consumed calcium carbonate was evaluated based on the mass loss between 600 and 800 °C on TGA curves of cement pastes studied (Figure 4). The consumed calcium carbonate normalized to the initial calcium carbonate content in ternary cement pastes is shown in Figure 5a–c. The consumed calcium carbonate increased with increasing curing and GGBFS content, as expected. From Figure 5a,b, it is clear that more calcium carbonate was consumed in cement pastes containing GOS at all ages. For example, in cement pastes containing GOS and after 3 days of hydration, 10% of consumed calcium carbonate was recorded for the P5GOS20BFS paste and more than 20% consumed calcium carbonate was recorded for the P5GOS30BFS paste. While in cement pastes containing LF, 9 and 17% of consumed calcium carbonate were recorded for the P5LF20BFS and the P5LF30BFS pastes, respectively. This might be attributed to the high reactivity of calcium carbonate present in GOS, which results in a better reaction of aluminate phases of GGBFS and thus, more carboaluminate phases were found. The higher consumption rate of calcium carbonate in cement pastes containing GOS might be also due to other reason in addition to the one mentioned above. Indeed, as mentioned in the Section 1, the content of calcium carbonate present in GOS is slightly higher than that of calcium carbonate present in LF. This means that the additional calcium carbonate from GOS results in more reaction of aluminate phases of GGBFS.

Figure 5c provides the consumed calcium carbonate for binary cement pastes prepared with GOS and LF (P5GOS and P5LF). A lower consumption rate of calcium carbonate was recorder for these mixes. The consumption rate of calcium carbonate in P5GOS was found to be respectively 5, 10 and 17% at 3, 7 and 28 days. Similarly, the consumption rate of calcium carbonate in P5LF was found to be 3, 5 and 17% at 3, 7 and 28 days, respectively. This means that the calcium carbonate present in GOS and LF also reacts with the aluminate phases of cement [26].

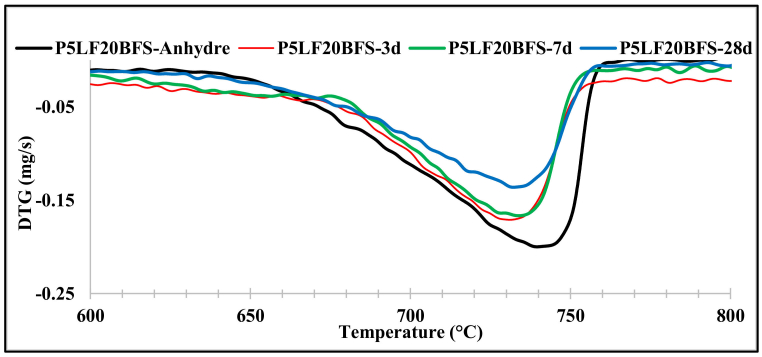

Figure 4. Consumption of calcium carbonate in cement pastes based on 5% LF and 20% BFS.

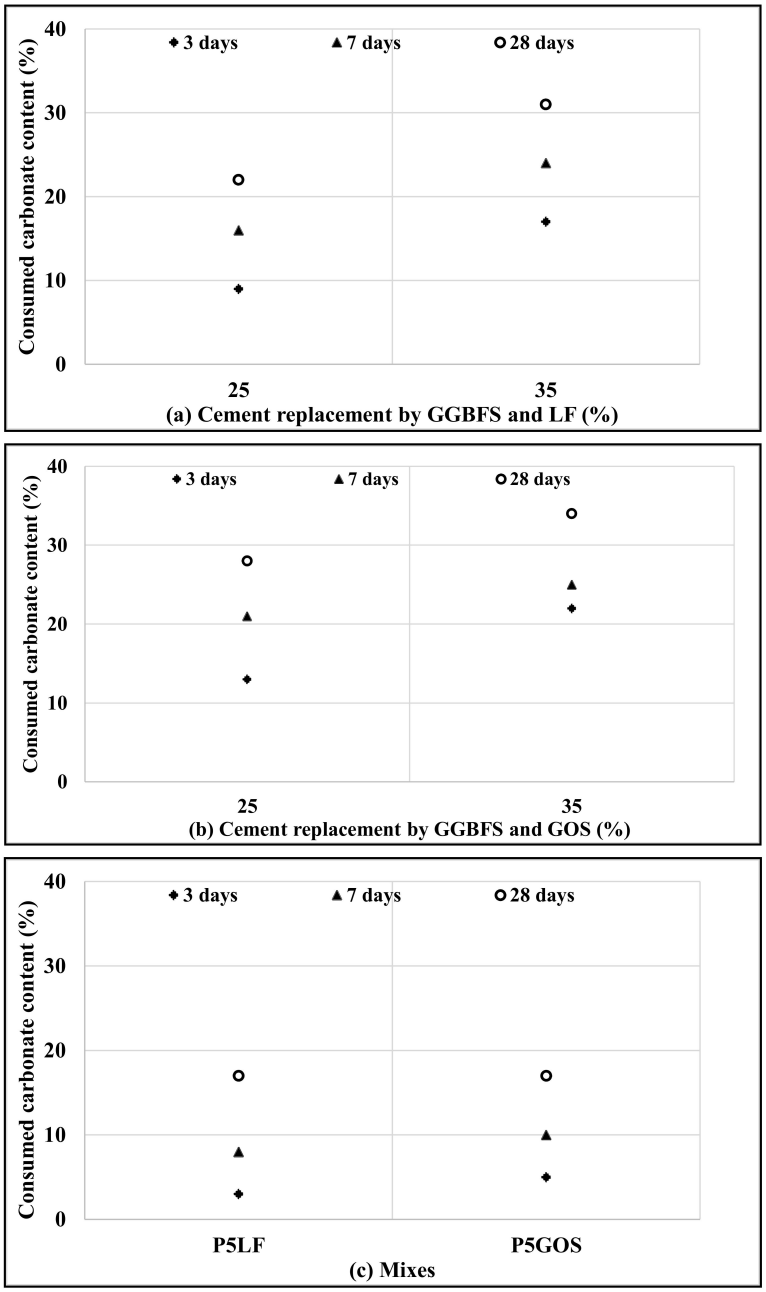

Figure 5. Normalized consumed calcium carbonate content of (**a**) cement pastes based on LF and GGBFS; (**b**) cement pastes based on GOS and GGBFS; (**c**) cement pastes based on LF or GOS.

3.4. Reaction Degree and Compressive Strength Development

To further establish the reactivity of calcium carbonate present in GOS and LF, which results in the formation of carboaluminate phases, the overall reaction degree of blended cement pastes, as well as the compressive strength, were determined.

Figure 6a,b provide the reaction degree development of binary and ternary cement pastes calculated using a methodology proposed in Refs. [27,37]. The reaction degree was estimated after 3, 7 and 28 days of hydration. It is clear from Figure 6a,b that the reaction degree for all cement pastes studied increased with increasing curing time as expected. In the case of binary blended cement paste where the Portland cement was replaced by 5% of GOS or LF, the reaction degree was slightly higher compared to that of reference cement paste at all ages. This firstly denotes the filler effect of GOS and LF on the cement hydration, but also the reaction of calcium carbonate present in these mineral additives with aluminate phase of cement. The cement paste based on GOS has a somewhat higher reaction degree compared to that of cement paste based on LF. Considering the 3 and 7 days of hydration, the reaction degree of P5LF was 8 and 4% higher, respectively, than the one of reference cement paste. Similarly, considering the 3 and 7 days of hydration, the reaction degree of P5GOS was slightly higher by about 8% compared to that of the reference cement paste. This indicates that the calcium carbonate present in GOS is more reactive compared to that present in LF, as indicated earlier.

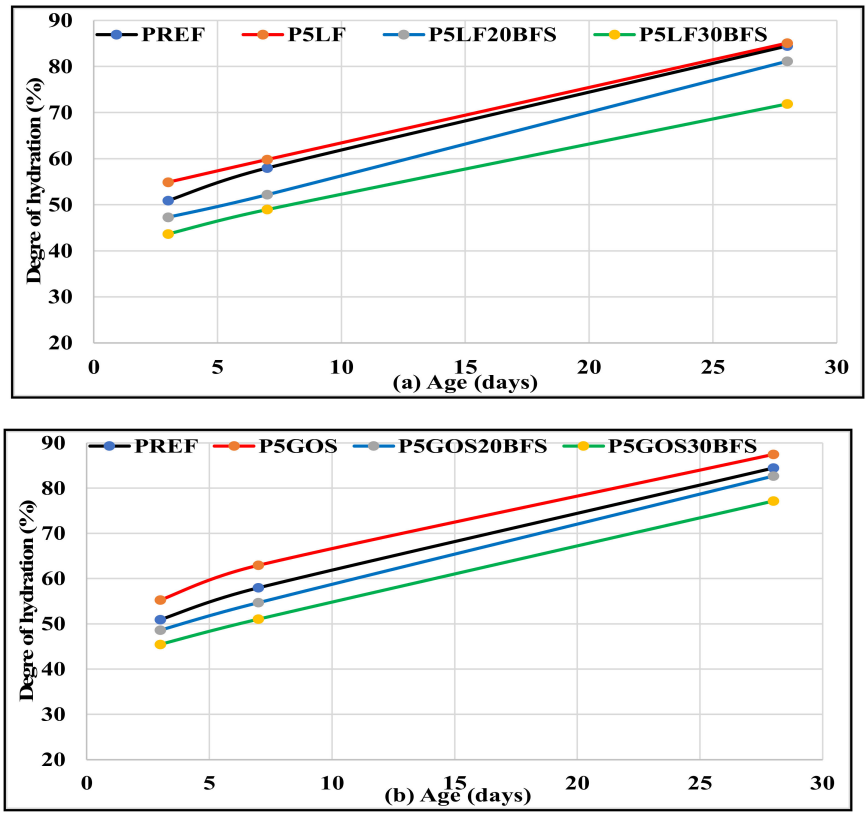

Figure 6. Overall reaction degree of (**a**) cement pastes based on LF and GGBFS; (**b**) cement pastes based on GOS and GGBFS.

In the case of ternary blended cement pastes where the Portland cement was replaced by both GGBFS and GOS or LF, the reaction degree was lower compared to that of reference cement paste. This is attributed to the dilution effect and to the slower reaction kinetics of GGBFS [37]. The cement pastes based on GGBFS and GOS, however, had a higher reaction degree at all ages compared to that of cement pastes based on GGBFS and LF. For example, the reaction degree of cement paste prepared with 5% GOS and 30% GGBFS was found

in the range of 45 and 77%. Meanwhile, the range of the reaction degree for cement paste prepared with 5% LF and 30% GGBFS was 43 and 63%. This confirms also that the calcium carbonate present in GOS is more reactive to that present in LF.

Compressive strength was further carried out to justify and verify the finding obtained. The compressive strength test was made on 4 cm-edge cubes after 3, 7 and 28 days as mentioned in Section 2.3.4.

Figure 7a,b provide the compressive strength results of the binary and ternary cement pastes studied in this study. The evolution of the compressive strength seems to match the corresponding overall reaction degree development where the compressive strength increased with increasing the overall reaction degree. The cement pastes containing GOS exhibited a higher compressive strength than the others cement pastes containing LF at all ages (3, 7 and 28 days). For example, the compressive strength exhibited by the cement paste containing 5% GOS and 30% GGBFS was found to be respectively, 18, 28 and 42 MPa at 3, 7 and 28 days. Meanwhile, the compressive strength exhibited by the cement paste containing 5% LF and 30% GGBFS was found to be respectively, 16, 28 and 37 MPa at 3, 7 and 28 days.

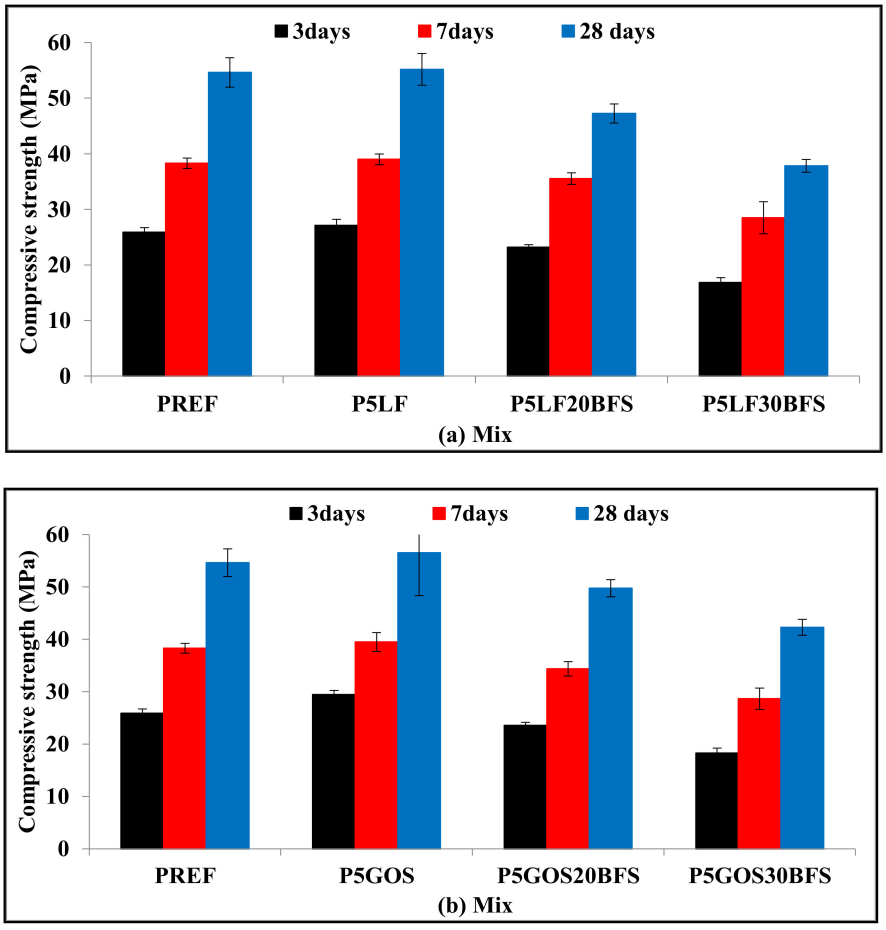

Figure 7. Compressive strength results. (**a**) cement pastes based on LF and GGBFS; (**b**) cement pastes based on GOS and GGBFS.

It is important to note here that the carboaluminate phases formation resulting from the interaction between carbonate calcium present in GOS or LF and aluminate phases originating from GGBFS cannot compensate the lower hydrate products of cement hydrates due to dilution effect [27], thus a lower overall reaction degree and compressive strength were observed in ternary cement pastes compared to that of reference cement paste.

4. Discussion

The results obtained by using different techniques to assess the formation of carboaluminate phases in binary and ternary blended cement pastes based on GGBFS, LF and GOS demonstrate that the calcium carbonate present in GOS is more reactive to that present in LF where higher hemi-and monocarboaluminates phases contents were observed in mixes based on GOS, particularly in ternary mixes. The higher reactivity of calcium carbonate present in GOS is attributed to the average diameters (apparent crystallite size ⟨D⟩) and the morphology of calcite particles. Indeed, the results from Rietveld refinement of calcium carbonate (Figure 8a,b) reveal that the average diameters of calcium carbonate particles present in GOS is about 1.7 times smaller compared to that present in LF (Table 3). The average diameters of calcium carbonate particles present in GOS and LF are 237 ± 5 and 403 ± 5 nm, respectively. Calcium carbonate particles present in GOS have far larger surface areas than the calcium carbonate particles present in LF. As the surface area increases, a greater amount of the calcium carbonate can come into contact with surrounding materials, thus improving the reactivity. Also, observations with a scanning electron microscope (SEM) for GOS and LF reveal that the GOS powder microstructure is observed as an arrangement of sheet layers of calcium carbonate, while LF particles exhibit angular shapes (Figure 9a,b). The arrangement as sheet layers of calcium carbonate of GOS causes more available space for hydrates growth.

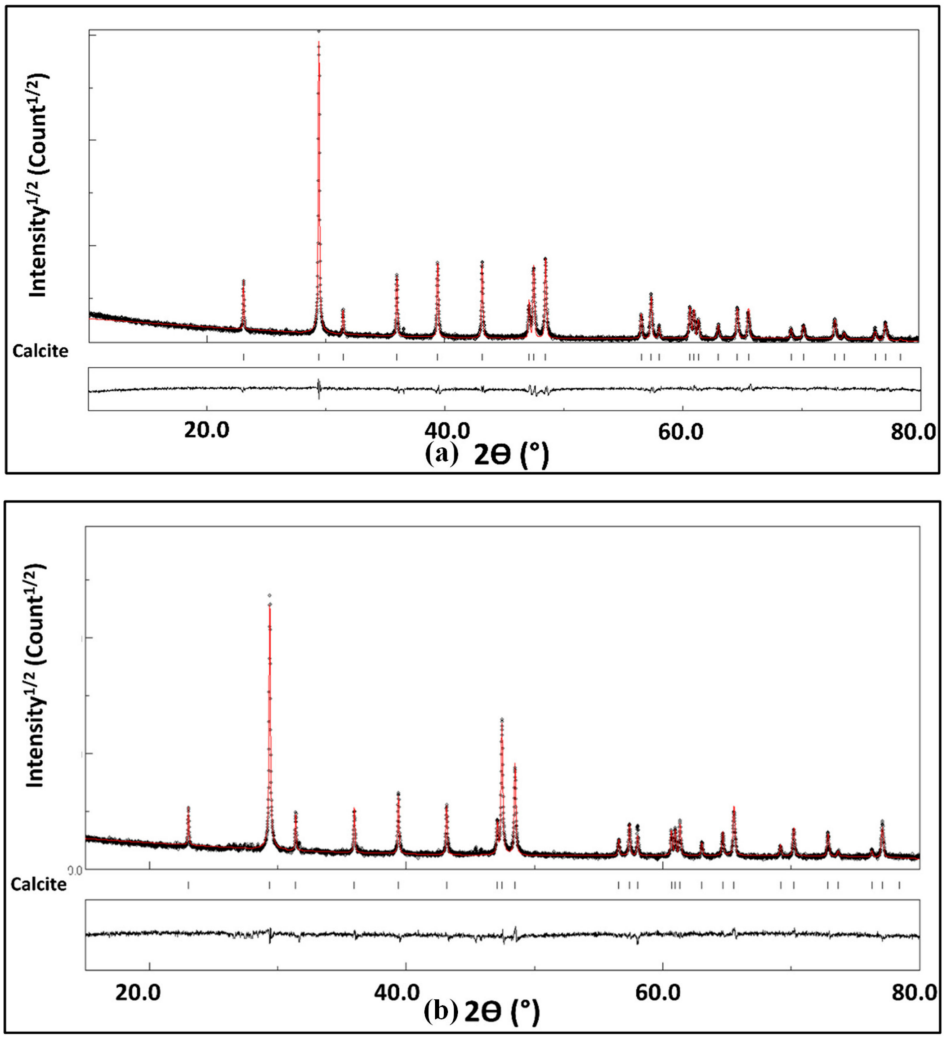

Figure 8. X-ray diffraction patterns of (**a**) LF and (**b**) GOS refined using the MAUD software. The calculated pattern (red line) is superimposed on the observed profile (coarse line). The difference curve (Iobs−Icalc) is shown at the bottom.

Table 3. Refined values of lattice parameters, unit cell volume, average diameter, microstrain <ε2>1/2, Standard deviations are indicated in parenthesis on the last digit.

Material	Phase	COD Reference	Lattice Type + Space Group	Lattice Parameters (Å)	⟨D⟩ (nm)	⟨ε2⟩1/2	Texture
LF	Calcite $CaCO_3$	1547347	Trigonal R-3c:H	a = 4.986 (1) c = 17.051 (2)	403 (20)	8. 10-4	Harmonic
GOS	Calcite $CaCO_3$	1547347	Trigonal R-3c:H	a = 4.989 (1) c = 17.077 (2)	237 (5)	5. 10-3	Harmonic

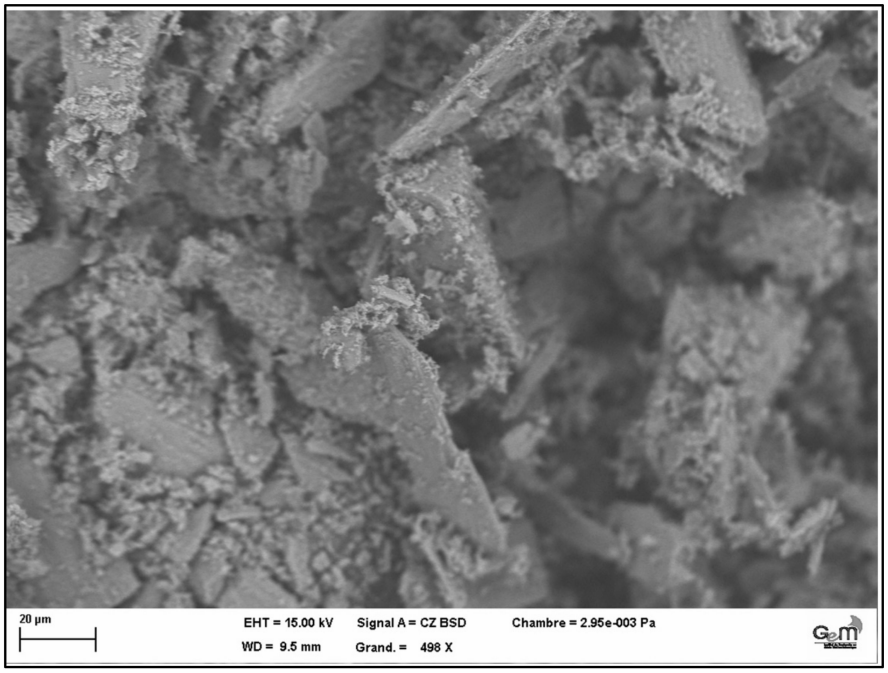

(**a**)

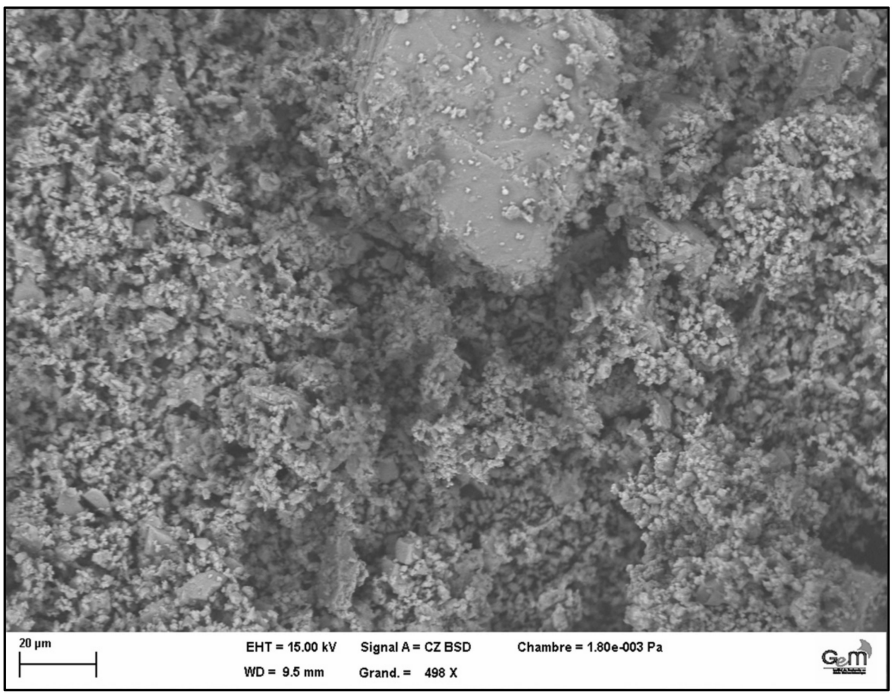

(**b**)

Figure 9. SEM images of (**a**) ground oyster shells; (**b**) limestone filler.

5. Conclusions

In this article, the reactivity effect of calcium carbonate present in LF or GOS on the formation of carboaluminate phases is presented. The presence of GOS and LF modified the hydration kinetics of both cement and GGBFS through their filler and activation effects. The calcium carbonate present in GOS and LF reacts with aluminate phases of GGBFS or cement to form hemi- and monocarboaluminate phases. based on the results obtained, and the observation made during the experimental tests using different techniques, the following conclusions may be drawn:

- The cement pastes containing 5% GOS exhibited a higher compressive strength and a higher overall reaction degree compared to that of cement pastes containing 5% LF, indicating the reactivity of calcium carbonate present in GOS.
- The aluminate phase's reaction followed using IC test and the consumed calcium carbonate calculated using TGA test confirmed that the calcium carbonate present in GOS reacts more with aluminate phases of GGBFS.
- The qualitative XRD analysis indicated that more hemi-and monocarboaluminate phases were formed in binary and ternary mixtures containing 5% GOS as cement replacement. Moreover, the qualitative XRD analysis indicated that the hemicarboaluminate formed firstly, followed by the monocarboaluminate phase.

The experimental results presented in this paper confirmed that the calcium carbonate present in GOS is more reactive compared to that present in LF. Hence, the GOS with high calcium carbonate reactivity has the potential to activate the hydration processes of GGBFS, particularly at early ages. Further studies on the effects of GGBFS and GOS contents however are needed to provide a better understanding of the effects of each material on the hydration kinetics.

Author Contributions: Conceptualization, W.D.; methodology, W.D.; software, Y.E.M.; validation, N.S.; investigation, W.D., Y.E.M., N.L., M.N.H., S.G. and A.F.; writing—original draft preparation, W.D.; writing—review and editing, W.D., N.S., Y.E.M., A.B. and U.J.A. All authors have read and agreed to the published version of the manuscript.

Funding: This research received no external funding.

Institutional Review Board Statement: Not applicable.

Informed Consent Statement: Not applicable.

Data Availability Statement: The data presented in the present paper are available from the corresponding author upon a reasonable request.

Conflicts of Interest: The authors declare no conflict of interest.

References

1. Barzgar, S.; Tarik, M.; Ludwig, C.; Lothenbach, B. The Effect of Equilibration Time on Al Uptake in C-S-H. *Cem. Concr. Res.* **2021**, *144*, 106438. [CrossRef]
2. Gartner, E. Industrially Interesting Approaches to "Low-CO2" Cements. *Cem. Concr. Res.* **2004**, *34*, 1489–1498. [CrossRef]
3. Zhao, Y.; Yu, M.; Xiang, Y.; Kong, F.; Li, L. A Sustainability Comparison between Green Concretes and Traditional Concrete Using an Emergy Ternary Diagram. *J. Clean. Prod.* **2020**, *256*, 120421. [CrossRef]
4. Song, Z.; Frühwirt, T.; Konietzky, H. Characteristics of Dissipated Energy of Concrete Subjected to Cyclic Loading. *Constr. Build. Mater.* **2018**, *168*, 47–60. [CrossRef]
5. Khan, S.; Maheshwari, N.; Aglave, G.; Arora, R. Experimental Design of Green Concrete and Assessing Its Suitability as a Sustainable Building Material. *Mater. Today Proc.* **2020**, *26*, 1126–1130. [CrossRef]
6. Wang, Y.; Tan, Y.; Wang, Y.; Liu, C. Mechanical Properties and Chloride Permeability of Green Concrete Mixed with Fly Ash and Coal Gangue. *Constr. Build. Mater.* **2020**, *233*. [CrossRef]
7. De Castro, S.; De Brito, J. Evaluation of the Durability of Concrete Made with Crushed Glass Aggregates. *J. Clean. Prod.* **2013**, *41*, 7–14. [CrossRef]
8. Jalal, M.; Nassir, N.; Jalal, H. Waste Tire Rubber and Pozzolans in Concrete: A Trade-off between Cleaner Production and Mechanical Properties in a Greener Concrete. *J. Clean. Prod.* **2019**, *238*. [CrossRef]

9. Teimortashlu, E.; Dehestani, M.; Jalal, M. Application of Taguchi Method for Compressive Strength Optimization of Tertiary Blended Self-Compacting Mortar. *Constr. Build. Mater.* **2018**, *190*, 1182–1191. [CrossRef]
10. Xuan, M.Y.; Han, Y.; Wang, X.Y. The Hydration, Mechanical, Autogenous Shrinkage, Durability, and Sustainability Properties of Cement–Limestone–Slag Ternary Composites. *Sustainability* **2021**, *13*, 1881. [CrossRef]
11. Panesar, D.K.; Zhang, R. Performance Comparison of Cement Replacing Materials in Concrete: Limestone Fillers and Supplementary Cementing Materials—A Review. *Constr. Build. Mater.* **2020**, *251*, 118866. [CrossRef]
12. Aqel, M.; Panesar, D.K. Hydration Kinetics and Compressive Strength of Steam-Cured Cement Pastes and Mortars Containing Limestone Filler. *Constr. Build. Mater.* **2016**, *113*, 359–368. [CrossRef]
13. Lothenbach, B.; Scrivener, K.; Hooton, R.D. Supplementary Cementitious Materials. *Cem. Concr. Res.* **2011**, *41*, 1244–1256. [CrossRef]
14. Deboucha, W.; Leklou, N.; Khelidj, A.; Plé, O.; Alengaram, U.J. Combination Effect of Limestone Filler and Slag on Delayed Ettringite Formation in Heat-Cured Mortar. *J. Mater. Civ. Eng.* **2020**, *32*, 04019365. [CrossRef]
15. Deboucha, W.; Leklou, N.; Khelidj, A. Blast Furnace Slag Addition Effects on Delayed Ettringite Formation in Heat-Cured Mortars. *KSCE J. Civ. Eng.* **2018**, *22*, 3484–3490. [CrossRef]
16. Salvador, R.P.; Rambo, D.A.S.; Bueno, R.M.; Silva, K.T.; De Figueiredo, A.D. On the Use of Blast-Furnace Slag in Sprayed Concrete Applications. *Constr. Build. Mater.* **2019**, *218*, 543–555. [CrossRef]
17. Ren, J.; Guo, S.-Y.; Qiao, X.-L.; Zhao, T.-J.; Zhang, L.-H.; Chen, J.-C.; Wang, Q. A Novel Titania/Graphene Composite Applied in Reinforcing Microstructural and Mechanical Properties of Alkali-Activated Slag. *J. Build. Eng.* **2021**, *41*. [CrossRef]
18. Wei, X.; Li, D.; Ming, F.; Yang, C.; Chen, L.; Liu, Y. Influence of Low-Temperature Curing on the Mechanical Strength, Hydration Process, and Microstructure of Alkali-Activated Fly Ash and Ground Granulated Blast Furnace Slag Mortar. *Constr. Build. Mater.* **2021**, *269*. [CrossRef]
19. Eren, Ö.; Yilmaz, Z. Strength Development of Conceretes with Ordinary Portland Cement, Partially Replaced by Slag or Fly Ash Cured at Different Temperatures 1 †. *Tek. Dergi* **2004**, *15*, 3311–3322.
20. Teng, S.; Lim, T.Y.D.; Divsholi, B.S. Durability and Mechanical Properties of High Strength Concrete Incorporating Ultra Fine Ground Granulated Blast-Furnace Slag. *Constr. Build. Mater.* **2013**, *40*, 875–881. [CrossRef]
21. He, T.; Li, Z.; Zhao, S.; Zhao, X.; Qu, X. Study on the Particle Morphology, Powder Characteristics and Hydration Activity of Blast Furnace Slag Prepared by Different Grinding Methods. *Constr. Build. Mater.* **2021**, *270*. [CrossRef]
22. Ghafari, E.; Ghahari, S.A.; Costa, H.; Júlio, E.; Portugal, A.; Durães, L. Effect of Supplementary Cementitious Materials on Autogenous Shrinkage of Ultra-High Performance Concrete. *Constr. Build. Mater.* **2016**, *127*, 43–48. [CrossRef]
23. Sebaibi, N.; Boutouil, M. Reducing Energy Consumption of Prefabricated Building Elements and Lowering the Environmental Impact of Concrete. *Eng. Struct.* **2020**, *213*, 110594. [CrossRef]
24. Li, C.; Jiang, L. Utilization of Limestone Powder as an Activator for Early-Age Strength Improvement of Slag Concrete. *Constr. Build. Mater.* **2020**, *253*. [CrossRef]
25. Arora, A.; Sant, G.; Neithalath, N. Ternary Blends Containing Slag and Interground/Blended Limestone: Hydration, Strength, and Pore Structure. *Constr. Build. Mater.* **2016**, *102*, 113–124. [CrossRef]
26. Adu-Amankwah, S.; Zajac, M.; Stabler, C.; Lothenbach, B.; Black, L. Influence of Limestone on the Hydration of Ternary Slag Cements. *Cem. Concr. Res.* **2017**, *100*, 96–109. [CrossRef]
27. Deboucha, W.; Leklou, N.; Khelidj, A. Combination Effect of Limestone Filler and Slag on Hydration Reactions in Ternary Cements. *Eur. J. Environ. Civ. Eng.* **2020**. [CrossRef]
28. Naqi, A.; Siddique, S.; Kim, H.K.; Jang, J.G. Examining the Potential of Calcined Oyster Shell Waste as Additive in High Volume Slag Cement. *Constr. Build. Mater.* **2020**, *230*. [CrossRef]
29. Mo, K.H.; Alengaram, U.J.; Jumaat, M.Z.; Lee, S.C.; Goh, W.I.; Yuen, C.W. Recycling of Seashell Waste in Concrete: A Review. *Constr. Build. Mater.* **2018**, *162*, 751–764. [CrossRef]
30. Liu, R.; Chen, D.; Cai, X.; Deng, Z.; Liao, Y. Hardened Properties of Mortar Mixtures Containing Pre-Treated Waste Oyster Shells. *J. Clean. Prod.* **2020**, *266*, 121729. [CrossRef]
31. Chen, D.; Zhang, P.; Pan, T.; Liao, Y.; Zhao, H. Evaluation of the Eco-Friendly Crushed Waste Oyster Shell Mortars Containing Supplementary Cementitious Materials. *J. Clean. Prod.* **2019**, *237*, 117811. [CrossRef]
32. Eziefula, U.G.; Ezeh, J.C.; Eziefula, B.I. Properties of Seashell Aggregate Concrete: A Review. *Constr. Build. Mater.* **2018**, *192*, 287–300. [CrossRef]
33. Her, S.; Park, T.; Zalnezhad, E.; Bae, S. Synthesis and Characterization of Cement Clinker Using Recycled Pulverized Oyster and Scallop Shell as Limestone Substitutes. *J. Clean. Prod.* **2021**, *278*. [CrossRef]
34. Bouasria, M.; Khadraoui, F.; Benzaama, M.-H.; Touati, K.; Chateigner, D.; Gascoin, S.; Pralong, V.; Orberger, B.; Babouri, L.; El Mendili, Y. Partial Substitution of Cement by the Association of Ferronickel Slags and Crepidula Fornicata Shells. *J. Build. Eng.* **2021**, *33*, 101587. [CrossRef]
35. Kuo, W.-T.; Wang, H.-Y.; Shu, C.-Y.; Su, D.-S. Engineering Properties of Controlled Low-Strength Materials Containing Waste Oyster Shells. *Constr. Build. Mater.* **2013**, *46*, 128–133. [CrossRef]
36. Zhong, B.-Y.; Zhou, Q.; Chan, C.-F.; Yu, Y. Structure and Property Characterization of Oyster Shell Cementing Material. *Chin. J. Struct. Chem.* **2012**, *31*, 85–92.

37. Deboucha, W.; Leklou, N.; Khelidj, A.; Oudjit, M.N. Hydration Development of Mineral Additives Blended Cement Using Thermogravimetric Analysis (TGA): Methodology of Calculating the Degree of Hydration. *Constr. Build. Mater.* **2017**, *146*, 687–701. [CrossRef]
38. European standard EN, N.F. 196-1. In *Méthodes d'essais Des Ciments-Partie 1: Détermination Des Résistances*; Association Française de Normalisation: Paris, France, 2016.
39. Caglioti, G.; Paoletti, A.T.; Ricci, F.P. Choice of Collimators for a Crystal Spectrometer for Neutron Diffraction. *Nucl. Instrum.* **1958**, *3*, 223–228. [CrossRef]
40. Gražulis, S.; Daškevič, A.; Merkys, A.; Chateigner, D.; Lutterotti, L.; Quiros, M.; Serebryanaya, N.R.; Moeck, P.; Downs, R.T.; Le Bail, A. Crystallography Open Database (COD): An Open-Access Collection of Crystal Structures and Platform for World-Wide Collaboration. *Nucleic Acids Res.* **2012**, *40*, D420–D427. [CrossRef]
41. Lutterotti, L.; Matthies, S.; Wenk, H.-R.; Schultz, A.S.; Richardson, J.W., Jr. Combined Texture and Structure Analysis of Deformed Limestone from Time-of-Flight Neutron Diffraction Spectra. *J. Appl. Phys.* **1997**, *81*, 594–600. [CrossRef]
42. European standard EN, N.F. 206-1. In *Béton—Partie 1: Spécification, Performances, Production et Conformité*; Association Française de Normalisation: Paris, France, 2004; p. 206.